Partial wetting of water on ice

Menno Demmenie,[1,2] Benjamin Gorin,[1,3] Paul Kolpakov,[1] Scott Smith,[1] Hamid Kellay,[3] and Daniel Bonn[1]

[1]*Institute of Physics, University of Amsterdam, Science Park 904, 1098 XH Amsterdam, the Netherlands*

[2]*Van 't Hoff Institute for Molecular Sciences, University of Amsterdam, Science Park 904, 1098XH Amsterdam, The Netherlands*

[3]*Laboratoire Ondes et Matière d'Aquitaine, Université de Bordeaux, 33400 Talence, France*

(Received 10 July 2024; accepted 17 April 2025; published 15 May 2025)

Is ice always covered by a thin layer of water? This question has been discussed for over 150 years. Here we show that the apparent contact angle of a droplet of water on ice increases steeply with decreasing ice temperature, from around 12 degrees near the melting point, to close to 160 degrees at −100°C. This indicates that ice is never completely wetted. We quantitatively model the temperature dependence of the apparent contact angle by assuming the droplet's contact line gets pinned due to the crystallization of a thin layer of ice on the cold surface. However close to the melting temperature, where the formation of the ice layer is slowest, surface energy considerations need to be included to explain the nonzero contact angle observed in experiments.

DOI: 10.1103/PhysRevFluids.10.054002

I. INTRODUCTION

The exploration of the wettability of ice crystals by water dates back to 1860, when Faraday used one of his famous Christmas lectures to report that ice cubes merge together at temperatures just below the melting temperature T_m [1], from which he concluded that there was a liquid water layer present on the ice cubes. More than 150 years later, the presence of a liquid layer on the surfaces of ice crystals is still under debate. The surface layer of ice is often referred to as a quasi-liquid-layer, with predicted thicknesses ranging from a few molecules to several hundreds of molecules [2,3].

The presence of such a layer, if the surface is really liquidlike, would imply complete wetting of the ice surface, in other words a liquid/solid contact angle of 0°. Past efforts to calculate the theoretical contact angle by considering the van der Waals forces at play in the air/water/ice system yielded values from 1° to 3.5° [4,5]. At the same time, experimental investigations yielded contact angles from 0° (complete wetting) to 40° (partial wetting) for sessile droplets on ice temperatures close to the melting temperature [6–12]. There is a lot of uncertainty on the nature of these reported angles, given that they were measured under nonequilibrium conditions [13]. In particular, the question remains to what extent crystallization influences contact line pinning, and to what extent the equilibrium between surface energies, as described by Young's equation, is obeyed.

In this work we combine three experimental approaches to reveal a nonzero apparent contact angle between the solid-liquid and the liquid-vapor interface. We model these observations based on the crystallization of a thin layer of ice that arrests droplet spreading. For temperatures close to T_m, where crystallization is slowest, Young's equation does need to be considered in order to

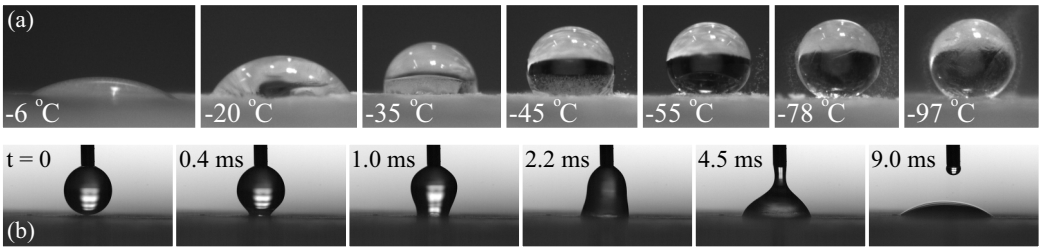

FIG. 1. (a) 5 μL demineralized sessile water droplets on ice surfaces at various temperatures (decreasing, from left to right, from −6°C to −97°C). Apparent contact angles increase with decreasing ice temperature from 12° to 160°. (b) Spreading dynamics of a 5 μL demineralized sessile water droplet on an ice surface of −6 °C. After about 9 ms, its contact line becomes pinned, effectively ending the spreading process.

obtain agreement with experimental observations, and reveals that water only partially wets ice. Our empirical model explains the observed wetting behavior and provides a more complete picture of the surface energy of ice, independently of the presence or absence of a surface layer.

II. METHODS

We first study the apparent contact angles of sessile water droplets [5 μL each, Fig. 1(a)] on planar ice surfaces at temperatures ranging from 172 to 272.5 K. Static sessile drops of 5 μL at room temperature were deposited onto ice with surface temperatures between −0.5°C and −101°C. A typical example is shown in Fig. 1(b). The experiments were carried out using an EasyDrop Kruss GmbH in a humidity controlled environment. The humidity was regulated by an inflow of nitrogen gas and monitored by a Thermo/Hygrometer (Testo 645). The parameters presented by Murphy and Koop were used to calculate the humidity required for vapor pressure equilibrium, minimizing the potential effects of frost formation [14]. Equilibrium conditions could be maintained down to ice temperatures of around −20 °C. Droplets of ultra purified water (Milli-Q) were illuminated by an external light source from the top to enhance contrast. Monothermal ice layers were formed on top of a copper plate (560 x 380 x 40 mm) and made of ultra purified water as well. Ice temperatures down to −30°C were achieved by a Peltier element (connected to BaseTech BT-305), which was placed underneath the copper plate and treated with thermal grease. The opposite, hot side of the Peltier element, was cooled by a flow of cooling agent. Temperatures below −30°C were achieved by a flow of liquid nitrogen (Norhof microdosing LN2, 900 series) instead of cooling agent. Droplets were brought in contact with the ice layer by moving the stage, to which the copper was attached, upwards with a velocity of approximately 0.5 mm/s in order to minimize the effect of impact on droplet spreading. To analyze spreading dynamics between the moment of deposition and the establishment of contact line pinning, a similar setup was used with a high-speed camera (Phantom TMX 7510) to determine arrest times close to the melting temperature, both on ice or a cold borosilicate glass substrate.

To confirm the nonzero plateau value of the contact angle near T_m, we also perform contact measurements on nonsessile droplets, using two techniques. Firstly, we advance and recede a cylinder of ice into and from a water bath, measuring the advancing and receding contact angles. Three cycles of advancing and receding are shown in Fig. 2, yielding consistent results. Ice rods with a diameter of 3.175 cm were prepared using a mold and filtered, double-boiled water, which was frozen at −15 °C. The water bath was maintained at a temperature just above T_m. Rods were immersed and withdrawn at velocities of several millimeters per second, with the results showing no dependence on speed within this range. We observe an advancing contact angle θ_a of 12°, and the receding contact angle θ_r stabilizes at a value of approximately 7°. These values were analyzed using the ImageJ contact angle tool. Secondly, we perform contact angle measurements on droplets

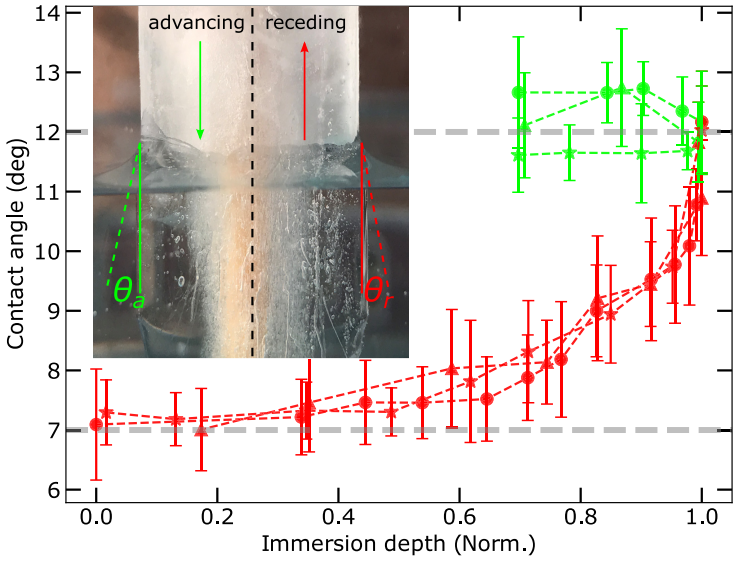

FIG. 2. Three advancing and receding contact angle hysteresis curves from immersed ice rod experiments into a water bath at a temperature of about 0.2 °C. Stars, triangles, and spheres depict three distinct measurements, with advancing contact angles in green and receding contact angles in red. Normalization is done by dividing the immersion or withdrawal depth by the maximum depth. As highlighted by two dashed grey lines, θ_a and θ_r plateau at angles of about 12° and 7°, respectively. Inset shows two snapshots taken from one of the experiments. Contact angles are measured at the liquid-solid interface.

moving on tilted ice surfaces at −15°C with inclinations ranging from 0° to 16°. These dynamically established contact angles (see Supplemental Material, Fig. S1 [15]) also yield a 12° advancing contact angle and a 7° receding contact angle close to T_m.

III. RESULTS AND DISCUSSION

In Fig. 3, the evolution of the droplet diameter as a function of time after deposition is shown for both ice and glass surfaces near T_m. In both cases, the spreading process is arrested after about 9 ms, at which time we measure the contact angle θ. As shown in Fig. 4 for droplets on ice, this apparent contact angle increases as the surface temperature decreases, starting from 12° near T_m. Since the droplet attains this angle during its advancement, we achieve consistency with θ_a from experiments involving the immersion of an ice rod into a water bath (Fig. 2). Below −60°C, the measured contact angles saturate at around 160°, thus indicating that the droplets arrest in less than 9 ms. Note that we do not observe contact angles of 0° near melting as would be expected if the ice surfaces would be wetted by a thin layer of water.

To understand our observations, we consider that the spreading dynamics of a droplet on a surface are governed by the balance between the capillary pressure and the inertial pressure inside the drop [16]. Consequently, the diameter of the contact area increases according to [17]:

$$D(t) = \alpha \left(\frac{\gamma R}{\rho} t^2 \right)^{1/4}, \tag{1}$$

with γ the surface tension of the liquid, ρ the density, R the initial radius of the droplet, and t the spreading time from the moment of initial contact. The prefactor α is a system-dependent parameter. From the collapse of data in Fig. 3(a) for measurements conducted on $T_{ice} > -15$ °C, we find $\alpha \approx 2.4$, consistent with previous reported values [17]. Although α appears to deviate at lower

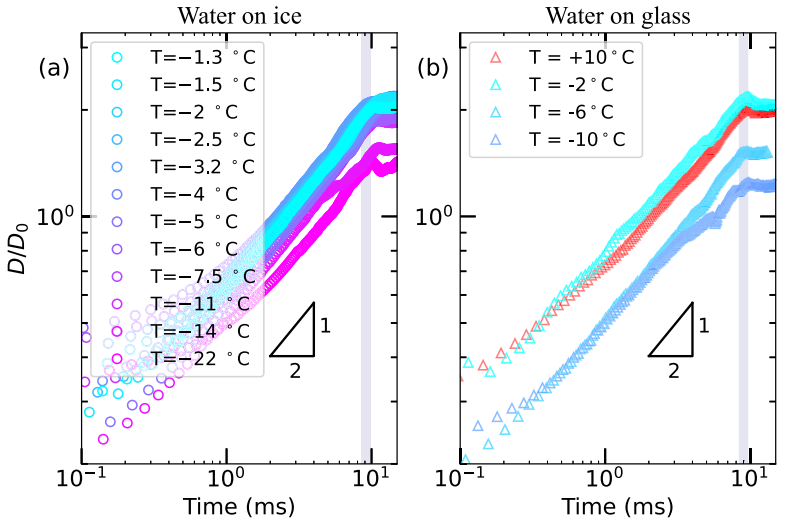

FIG. 3. Experimental measurements of contact diameter plotted as a function of time in the temperature regime close to T_m on ice (a) and glass (b). The contact diameter (D) on the y axis is rescaled by the initial diameter of the droplet before contact (D_0). Up to $t \approx 9$ ms (indicated by a grey line), the spreading dynamics are in agreement with Eq. (1), with $\alpha \approx 2.4$.

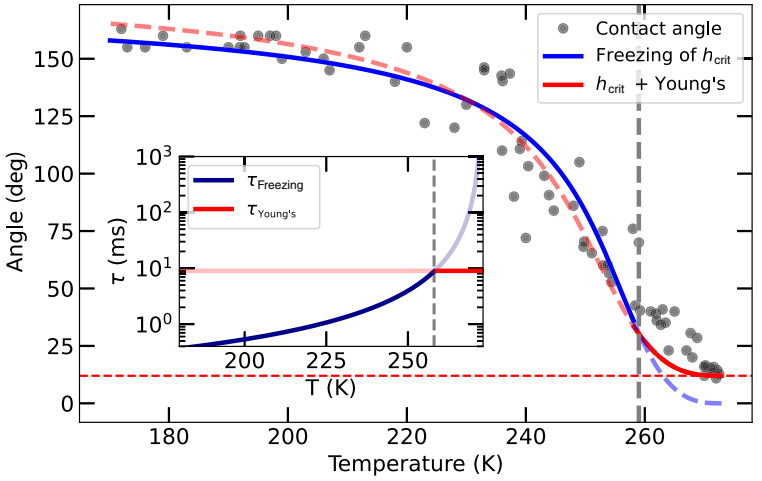

FIG. 4. Measured apparent contact angle of 5 µL sessile water droplets on ice as a function of ice temperature. The blue line depicts the fit for our model assuming contact line arrest as soon as crystallization near the surface reaches a critical layer thickness, fitted at $h_{\mathrm{crit}} = 10\,\mu\mathrm{m}$. Close to the melting temperature the model predicts an angle of 0° as the required time to form the critical ice layer diverges to infinity. Measured values however plateau at a frequently reported contact angle of 12°. The red line is the fit for a combination of an equilibrium contact angle of 12°, and our model with $h_{\mathrm{crit}} = 12\,\mu\mathrm{m}$. Inset shows the arrest time (τ) of a 5 µL droplet according to our ice formation model in blue and Young's equation in red. The shorter τ determines the dominant mechanism as depicted by the solid line in the main figure, with the crossover temperature around 259 K indicated by a dotted line. Sequential measurements conducted near T_m yielded error bars smaller than the corresponding data points.

temperatures, we treat it as a constant parameter in our model. We assume that the polycrystalline structure of ice has a negligible effect on droplet spreading, as both the entropy and enthalpy of different crystal facets exhibit nearly identical values [18]. Furthermore, friction measurements on polycrystalline ice yield results comparable to those obtained on monocrystalline ice [19]. Lolla *et al*. conducted droplet spreading experiments on ice with varying impact velocities and concluded that, for gently deposited droplets, the used capillary scaling law for the measured spreading radius remains valid [20]. However, at higher impact velocities, a second inertioviscous regime emerges when spreading extends beyond a frozen contact line [21].

When the surface temperature is lower than the melting temperature, the spreading of the contact line could certainly be arrested due to the freezing and subsequent pinning of the contact line. Previous studies, based on principles of Tavakoli *et al*. and Schiaffino and Sonin [22,23], have developed comprehensive models for the exact shape of the solidification front of liquid droplets on supercooled surfaces [24–27]. Grivet *et al*. demonstrated that dendritic crystals, growing with a constant velocity on an undercooled sapphire substrate, catch up with the spreading droplet [$D \propto \sqrt{t}$, Eq. (1)] and consequently cause pinning events [28]. Since our focus is on the macroscopic apparent contact angle on ice specifically, we do not expect sufficient undercooling at the surface, and thus no dendrites to form. Gorin *et al*. showed that these models fail to accurately describe the final apparent contact angles of droplets, especially at low impact velocities. To address this limitation, they proposed an empirical model to account for the contact angles by assuming a frozen layer. [29].

To comprehend the final apparent contact angle of a water droplet on a cold ice surface, we adopt the model of Gorin *et al*. and posit that droplet spreading could be arrested once an ice layer of thickness h exceeds a critical threshold h_{crit}, thereby limiting the maximum spreading radius. In our analysis, we use the contact angle as the primary observable, which is related to the maximum spreading radius through the assumption of volume conservation and reshaping of the droplet into a spherical cap. This value depends upon the thermal properties of the liquid and the substrate and is treated as a free fitting parameter. The freezing dynamics inside the droplet are determined from the analytical solution of the Stefan problem (see Supplemental Material [15]), which yields the time evolution of the ice layer thickness:

$$h(t) = \sqrt{C(T) \cdot t}, \tag{2}$$

with $C(T)$ a constant depending on the thermal properties of the liquid droplet and solid surface. Combining Eq. (2) with h_{crit}, we find for the time of contact line arrest due to freezing:

$$\tau_{\text{freezing}} = \frac{{h_{\text{crit}}}^2}{C(T)}. \tag{3}$$

Then, we deduce the final spreading diameter by substituting the time (t) in Eq. (1) with τ_{freezing}:

$$D_{\text{end}} = D(\tau_{\text{freezing}}) = \alpha \left(\frac{\gamma R}{\rho} \frac{{h_{\text{crit}}}^4}{C(T)^2} \right)^{1/4}. \tag{4}$$

Finally, the apparent contact angle θ_{end} is determined under the assumption that the droplet maintains its volume and reshapes into a spherical cap (more details in Supplemental Material [15]):

$$\theta = 90 - \arccos\left(\frac{H \cdot D_{\text{end}}}{H^2 + \frac{1}{4} D_{\text{end}}^2} \right), \text{ if } \theta < 90^\circ, \tag{5a}$$

$$\theta = 90 + \arccos\left(\frac{H \cdot D_{\text{end}}}{H^2 + \frac{1}{4} D_{\text{end}}^2} \right), \text{ if } \theta > 90^\circ, \tag{5b}$$

with H the theoretical height of the spherical cap. In this form, the model fits to a certain degree with the experimental values (blue curve in Fig. 4). However, a notable discrepancy emerges for $T \to T_m$:

the model, as well as all previously proposed models, underestimates the measured contact angles. This discrepancy could be intuitively understood by the fact that, as the temperature approaches T_m, the freezing time (τ_{freezing}) required to form h_{crit}, diverges towards infinity. Hence, the predicted apparent contact angle converges towards 0°. To overcome this mismatch, we will introduce an additional empirical term.

As shown in Fig. 3(a), the arrest time of 5 μL droplets deposited on ice at temperatures close to T_m is about 9 ms. This is shorter than the timeframe that can be explained by pinning due to the crystallization of h_{crit}. In other words, crystallization of h_{crit} is too slow to pin the droplet near T_m. Hence, in this temperature regime, the contact angle must be a result of an equilibrium in surface energies; i.e., Young's law. In order to find a particular crossover temperature (T_c) above which Young's arrest plays a role we equate the maximum arrest time of 9 ms ($\tau_{\text{Young's}}$) with the one calculated via Eq. (3) (τ_{freezing}):

$$\tau_{\text{Young's}} = \tau_{\text{freezing}}(T). \tag{6}$$

In the inset of Fig. 4 we present a graphical representation of Eq. (6), revealing that $T_c = 259$ K. Hence, below this crossover temperature, the apparent contact angle is fully determined by contact pinning due to the crystallization of an ice layer of height h_{crit}. Above this temperature, the predicted final diameter of the droplet (D_{end}) diverges to infinity, and does not accurately describe the experimentally obtained values (See Supplemental Material, Fig. S2 [15]). Therefore we introduce an additional contact angle of 12° for $T_{\text{ice}} > T_c$. This aligns with earlier findings that demonstrate a linear relationship between the measured contact angle and $1/\gamma_{lv}$ near T_m, indicating that a Young's equilibrium is indeed responsible for establishing the contact angle [10]. Thus, the final expression for apparent contact angles of water drops on a planar ice surface becomes

$$\theta = 90 \pm \arccos\left(\frac{H \cdot D_{\text{end}}}{H^2 + \frac{1}{4}D_{\text{end}}^2}\right), \text{ if } T < T_c, \tag{7a}$$

$$\theta = 90 \pm \arccos\left(\frac{H \cdot D_{\text{end}}}{H^2 + \frac{1}{4}D_{\text{end}}^2}\right) + 12, \text{ if } T > T_c. \tag{7b}$$

Here, the ± should be considered − when $\theta < 90°$, and + when $\theta > 90°$. The blue curve in Fig. 4 is based on Eq. (7a) with the empirical value $h_{\text{crit}} = 10$ μm. Above T_c, the red curve based on Eq. (7b), yields a nearly identical fitting value of $h_{\text{crit}} = 12$ μm. As a consequence, a discontinuity arises precisely at T_c.

Finally, the red curve [Eq. (7b)] in Fig. 4 accurately describes the plateau of 12°, but slightly underestimates the measured apparent contact angles between T_c and T_m. This discrepancy presumably occurs because we treated $\tau_{\text{Young's}}$ as a temperature-independent constant, neglecting slight indications of a decrease with decreasing temperature. Additionally, surface roughness, a parameter not considered in the model, is known to play a fundamental role in wetting theory [30–34]. Furthermore, frost formation on ice surfaces was observed at temperatures below approximately −20 °C as the required humidity levels fell below the capabilities of our setup. This may contribute to the variability in reported apparent contact angles within this temperature range. However, it does not affect the experiments conducted near T_m where finite contact angles result from Young's equilibrium, as vapor pressure equilibrium was successfully maintained.

For comparison, we conducted similar experiments involving sessile water droplets on cold borosilicate glass. In contrast to ice surfaces, it is feasible to measure contacts angles above T_m: we observe that the contact angle decreases with temperature in a similar fashion as observed for ice, with a clear plateau for $T > T_m$ of ≈28° (See Supplemental Material, Fig. S3 where the results are compared to the prediction of our model [15]). The fact that this plateau angle is different from that of an ice surface (≈12°) is consistent with the picture of the contact angle being determined by Young's law, which considers material-dependent surface energies.

IV. CONCLUSIONS

In conclusion, we studied the spreading of water droplets on ice surfaces ranging from 172 to 272.5 K, finding a minimum contact angle of 12° close to the melting temperature, increasing to about 160° at lower temperatures, indicating that the ice is not fully wetted by water. We find that below a crossover temperature T_c, droplet spreading is primarily governed by contact line arrest, where a thin layer of ice crystallizes, arresting the movement of the contact line when it exceeds a critical thickness on the order of 12 μm. However, above T_c, and close to T_m, a model based exclusively on crystallization fails to explain experimentally observed contact angles of about 12°, as the predicted apparent contact angle converges to 0°. Therefore, it becomes essential to incorporate the equilibrium between the surface energies of the solid, liquid and gas interfaces into the model, along with the corresponding Young's contact angle. These findings align with calculations of the Hamaker constant, where the presence of water in between air and ice results in attractive interactions [5,35].

The presence of a layer of water on the surface of ice has been inferred in the past to account for some of the specific properties of ice, such as its slipperiness and sintering behavior. Our measurements indicate that this layer is not. Recently it has in fact been suggested that slipperiness of ice is due to the the outermost molecular layer being highly mobile [19,36]; this ties in with the observation that scratches in ice spontaneously disappear [37]. The sintering was studied quantitatively also recently by observing how a wedge-shaped scratch made in ice closes up. It was shown that this self-healing property is in fact due to a rapid sublimation-condensation, i.e., transport through the vapor phase rather than the flow of a liquid layer [37,38]. The peculiarity of ice compared to other solids is then that the vapor pressure is very high (ice drops evaporate just as quickly as water drops [39]), leading to an interface with very mobile molecules. This, however, is not a liquid, as evidenced by the dynamics of scratch healing and the recently discovered viscoelastic properties [40], but is perhaps better characterized as a highly mobile 2D gas that exchanges molecules with the vapor phase. The presence of such a layer is then the reason for the nonzero contact angle of water on the surface.

ACKNOWLEDGMENT

This work is financially supported by NWO Projectruimte No. 680-91-133.

DATA AVAILABILITY

The data that support the findings of this article are not publicly available. The data are available from the authors upon reasonable request.

[1] M. Faraday, I. Note on regelation, Proc. R. Soc. London **10**, 440 (1860).
[2] B. Slater and A. Michaelides, Surface premelting of water ice, Nat. Rev. Chem. **3**, 172 (2019).
[3] Y. Li and G. A. Somorjai, Surface premelting of ice, J. Phys. Chem. C **111**, 9631 (2007).
[4] M. Elbaum and M. Schick, Application of the theory of dispersion forces to the surface melting of ice, Phys. Rev. Lett. **66**, 1713 (1991).
[5] J. Luengo-Márquez, F. Izquierdo-Ruiz, and L. G. MacDowell, Intermolecular forces at ice and water interfaces: Premelting, surface freezing, and regelation, J. Chem. Phys. **157**, 044704 (2022).
[6] C. A. Knight, The contact angle of water on ice, J. Colloid Interface Sci. **25**, 280 (1967).
[7] J. Drelich, E. Chibowski, D. D. Meng, and K. Terpilowski, Hydrophilic and superhydrophilic surfaces and materials, Soft Matter **7**, 9804 (2011).

[8] W. M. Ketcham and P. V. Hobbs, An experimental determination of the surface energies of ice, Philos. Mag. **19**, 1161 (1969).
[9] V. Thiévenaz, C. Josserand, and T. Séon, Retraction and freezing of a water film on ice, Phys. Rev. Fluids **5**, 041601(R) (2020).
[10] M. Demmenie, L. Reus, P. Kolpakov, S. Woutersen, D. Bonn, and N. Shahidzadeh, Growth and form of rippled icicles, Phys. Rev. Appl. **19**, 024005 (2023).
[11] Ken-ichiro Murata, H. Asakawa, K. Nagashima, Y. Furukawa, and G. Sazaki, Thermodynamic origin of surface melting on ice crystals, Proc. Natl. Acad. Sci. USA **113**, 1749 (2016).
[12] A. Huerre, C. Josserand, and T. Séon, Freezing and capillarity, Annu. Rev. Fluid Mech. **57**, 257 (2025).
[13] Y. Nagata, T. Hama, E. H. G. Backus, M. Mezger, D. Bonn, M. Bonn, and G. Sazaki, The surface of ice under equilibrium and nonequilibrium conditions, Acc. Chem. Res. **52**, 1006 (2019).
[14] D. M. Murphy and T. Koop, Review of the vapour pressures of ice and supercooled water for atmospheric applications, Q. J. R. Meteorol. Soc. **131**, 1539 (2005).
[15] See Supplemental Material at http://link.aps.org/supplemental/10.1103/PhysRevFluids.10.054002 for complementary experiments, including: Sessile droplet experiments on inclined ice planes; measurements of maximum droplet spreading diameter as a function of ice temperature; and sessile droplet behavior on cold glass surfaces. In addition, the full derivation of the final contact angle is provided, starting from the one-dimensional Stefan problem.
[16] K. G. Winkels, J. H. Weijs, A. Eddi, and J. H. Snoeijer, Initial spreading of low-viscosity drops on partially wetting surfaces, Phys. Rev. E **85**, 055301(R) (2012).
[17] A.-L. Biance, C. Clanet, and D. Quéré, First steps in the spreading of a liquid droplet, Phys. Rev. E **69**, 016301 (2004).
[18] M. J. Shultz, E. F. Gubbins, R. G. Davies, Z. Lin, and Z. Xiong, Ice interfaces: Vapor, liquid, and solutions, J. Phys. Chem. C **128**, 12326 (2024).
[19] B. Weber, Y. Nagata, S. Ketzetzi, F. Tang, W. J. Smit, H. J. Bakker, E. H. G. Backus, M. Bonn, and D. Bonn, Molecular insight into the slipperiness of ice, J. Phys. Chem. Lett. **9**, 2838 (2018).
[20] N. Laan, K. G. de Bruin, D. Bartolo, C. Josserand, and D. Bonn, Maximum diameter of impacting liquid droplets, Phys. Rev. Appl. **2**, 044018 (2014).
[21] V. Y. Lolla, S. F. Ahmadi, H. Park, A. P. Fugaro, and J. B. Boreyko, Arrested dynamics of droplet spreading on ice, Phys. Rev. Lett. **129**, 074502 (2022).
[22] S. Schiaffino and A. A. Sonin, Motion and arrest of a molten contact line on a cold surface: An experimental study, Phys. Fluids **9**, 2217 (1997).
[23] F. Tavakoli, S. H. Davis, and H. P. Kavehpour, Spreading and arrest of a molten liquid on cold substrates, Langmuir **30**, 10151 (2014).
[24] R. B. J. Koldeweij, P. Kant, K. Harth, R. de Ruiter, H. Gelderblom, J. H. Snoeijer, D. Lohse, and M. A. J. van Limbeek, Initial solidification dynamics of spreading droplets, Phys. Rev. Fluids **6**, L121601 (2021).
[25] R. de Ruiter, P. Colinet, P. Brunet, J. H. Snoeijer, and H. Gelderblom, Contact line arrest in solidifying spreading drops, Phys. Rev. Fluids **2**, 043602 (2017).
[26] R. Herbaut, J. Dervaux, P. Brunet, L. Royon, and L. Limat, A criterion for the pinning and depinning of an advancing contact line on a cold substrate, Eur. Phys. J.: Spec. Top. **229**, 1867 (2020).
[27] V. Thiévenaz, T. Séon, and C. Josserand, Solidification dynamics of an impacted drop, J. Fluid Mech. **874**, 756 (2019).
[28] R. Grivet, A. Monier, A. Huerre, C. Josserand, and T. Séon, Contact line catch up by growing ice crystals, Phys. Rev. Lett. **128**, 254501 (2022).
[29] B. Gorin, D. Bonn, and H. Kellay, Droplet impacts on cold surfaces, J. Fluid Mech. **944**, A23 (2022).
[30] D. Bonn, J. Eggers, J. Indekeu, J. Meunier, and E. Rolley, Wetting and spreading, Rev. Mod. Phys. **81**, 739 (2009).
[31] J. Wang, Y. Wu, Y. Cao, G. Li, and Y. Liao, Influence of surface roughness on contact angle hysteresis and spreading work, Colloid Polym. Sci. **298**, 1107 (2020).
[32] J. Bico, C. Tordeux, and D. Quéré, Rough wetting, Europhys. Lett. **55**, 214 (2001).
[33] C. Huh and S. G. Mason, Effects of surface roughness on wetting (theoretical), J. Colloid Interface Sci. **60**, 11 (1977).

[34] T. de Goede, K. de Bruin, N. Shahidzadeh, and D. Bonn, Droplet splashing on rough surfaces, Phys. Rev. Fluids **6**, 043604 (2021).
[35] J. Benet, P. Llombart, E. Sanz, and L. G. MacDowell, Structure and fluctuations of the premelted liquid film of ice at the triple point, Mol. Phys. **117**, 2846 (2019).
[36] R. W. Liefferink, F.-C. Hsia, B. Weber, and D. Bonn, Friction on ice: How temperature, pressure, and speed control the slipperiness of ice, Phys. Rev. X **11**, 011025 (2021).
[37] M. Demmenie, P. Kolpakov, Y. Nagata, S. Woutersen, and D. Bonn, Scratch-healing behavior of ice by local sublimation and condensation, J. Phys. Chem. C **126**, 2179 (2022).
[38] M. Demmenie, S. Woutersen, and D. Bonn, Ice sintering by sublimation and condensation, J. Phys. Chem. Lett. **16**, 2104 (2025).
[39] E. Jambon-Puillet, N. Shahidzadeh, and D. Bonn, Singular sublimation of ice and snow crystals, Nat. Commun. **9**, 4191 (2018).
[40] L. Canale, J. Comtet, A. Niguès, C. Cohen, C. Clanet, A. Siria, and L. Bocquet, Nanorheology of interfacial water during ice gliding, Phys. Rev. X **9**, 041025 (2019).